hydrology

MDPI

Article

The Rise of the Rare and Severe, an Unsupervised Dynamical Fingerprint of Heatwaves and Extreme Events of Precipitation over Italy from 1991 to 2020

Matteo Gentilucci [1,*], Hamed Younes [2,3], Rihab Hadji [4] and Gilberto Pambianchi [5]

[1] School of Biosciences and Veterinary Medicine, University of Camerino, 62032 Camerino, Italy
[2] Laboratory for the Application of Materials to the Environment, Department of Earth Sciences, Water and Energy, LAM3E, University of Gafsa, Gafsa 2100, Tunisia; hamed.younes@fsgafsa.rnu.tn
[3] Department of Earth and Atmospheric Sciences, University of Houston, Houston, TX 77204, USA
[4] Department of Earth Sciences, Institute of Architecture and Earth Sciences, Setif 1 University, Setif 19000, Algeria; rihab.hadji@univ-setif.dz
[5] Geology Division, School of Science and Technology, University of Camerino, 62032 Camerino, Italy; gilberto.pambianchi@unicam.it
* Correspondence: matteo.gentilucci@unicam.it

Abstract

Extreme heat and extreme rainfall are usually described by point-based indices, such as counts of threshold-exceedance days or annual maxima, which do not capture how events evolve in space and time. This study proposes an event-based framework that tracks heatwaves and extreme precipitation over Italy as three-dimensional (latitude–longitude–time) objects, using hourly ERA5 reanalysis data (0.25°) aggregated to daily values for the 1991–2020 WMO climatological standard normal period. Candidate extremes were identified with conventional percentile thresholds and linked through 26-connectivity labelling. Each event was described by eight dynamical features and classified by K-means clustering, with the number of clusters chosen with the aid of silhouette analysis. The 1767 heatwaves were grouped into brief localised spikes, regional multi-day heatwaves and persistent nationwide heatwaves (silhouette score 0.32, weak-to-moderate separation), and the 10,925 extreme precipitation events into local bursts, persistent quasi-stationary systems and organised propagating systems (silhouette score 0.66). In both hazards, only the rarest and physically most extreme archetype showed a statistically significant increase in annual frequency, although for precipitation local bursts showed a borderline increase ($p = 0.07$). Persistent nationwide heatwaves rose from about three to about ten events per year (Kendall's $\tau = 0.69$, $p < 0.0001$), with significant local increases over 97% of the grid cells. Organised propagating systems nearly doubled ($\tau = 0.43$, $p = 0.0017$), with significant local increases in 9% of the grid cells, mainly over the Ligurian Sea and western Sardinia, the central Apennines and Calabria–north-eastern Sicily. Changes in Italian extremes during 1991–2020 were therefore concentrated in specific event types rather than uniform across them. The framework is potentially transferable to other climatically heterogeneous regions.

Keywords: extreme precipitation; heatwaves; unsupervised classification; event tracking; object-based analysis; ERA5 reanalysis; climate change; Italy; spatiotemporal clustering; Mediterranean hydrometeorological hazards

Check for updates

Academic Editor: Xander Wang

Received: 25 September 2026
Revised: 14 November 2026
Accepted: 20 November 2026
Published: 25 November 2026

Copyright: © 2026 by the authors. Licensee MDPI, Basel, Switzerland. This article is an open access article distributed under the terms and conditions of the Creative Commons Attribution (CC BY) license.

1. Introduction

Weather and climate extremes are now the dominant channel through which society experiences climate change. The Sixth Assessment Report of the Intergovernmental Panel

on Climate Change concludes with high confidence that the frequency and intensity of hot extremes and heavy precipitation have increased over most land areas since the 1950s, and that these changes will continue under every considered emission scenario [1]. The Mediterranean basin is repeatedly identified as one of the regions most responsive to this forcing: it combines a pronounced warming signal with a projected reduction in mean precipitation and an increase in the intensity of the rainfall that does occur [2,3]. Italy, at the centre of this basin, adds a further layer of complexity. The country spans more than twelve degrees of latitude, from Alpine peaks above 4000 m in the north to the subtropical coastal plains of Sicily. Within a single national territory, it therefore includes continental, Mediterranean and semi-arid climate types [4,5]. Understanding how extremes behave across this heterogeneous domain, and how their behaviour is changing, is therefore both a scientific and a societal priority.

The societal cost of these extremes is already visible. Heatwaves are associated with sharp increases in all-cause mortality among the elderly, and Italy has the oldest population in the European Union [6]. National surveillance, based on the heatwave prevention plan of the Italian Ministry of Health and on remote sensing indicators, has recorded an increasing number of extreme heat days and of heatwave-related excess mortality episodes in recent summers. In this respect, 2022 and 2023 stand out as exceptional years [6,7]. On the precipitation side, short, intense and often localised rainfall events have caused some of the most damaging natural disasters in recent Italian history. During the Marche–Umbria flood of 15–16 September 2022, nearly 420 mm of rain fell in six hours over a catchment of about 5000 km^2, triggering widespread landslides and causing thirteen fatalities [8,9]. Comparable events have repeatedly struck Liguria, the Adriatic side of the Apennines and the alluvial fans of the Po valley [10,11].

Most of the available evidence on changes in these extremes comes from fixed, point-based indices. The Expert Team on Climate Change Detection and Indices (ETCCDI) defined a widely used set of descriptors, including the number of days exceeding a fixed or percentile-based threshold, the annual maximum one-day and five-day precipitation totals, and the fraction of annual precipitation falling on very wet days [12]. For heat, the most established descriptor is the Heat Wave Magnitude Index daily (HWMId), which defines a heatwave as at least three consecutive days with maximum temperature above the local 90th percentile and integrates the exceedance over the event into a single magnitude value [13,14]. When these indices are applied to Italy, the picture is consistent for temperature but more contrasting for precipitation. Station-based studies agree on long-term warming and on a rise in extreme heat days across the peninsula [15,16]. For precipitation, studies based on dense rain gauge networks, high-resolution gridded datasets, satellite products and reanalyses report trends in the intensity of the wettest days that are generally positive but strongly heterogeneous in space: many areas show no significant change, whereas a minority show significant intensification, often concentrated in specific orographic or coastal corridors [17–21]. Libertino et al. [21] concluded that evidence for increasing rainfall extremes remains elusive when Italy is analysed at large spatial scales, whereas analyses at regional or sub-daily scales more often detect intensification [19]. Extreme value analyses point in the same direction. In central Italy, return levels of the generalised extreme value distribution estimated from recent, shorter sub-periods can exceed those estimated from the full historical record, a symptom of non-stationarity in the underlying process [9,22–24], and comparable non-stationary behaviour has been documented at sub-daily resolution in the Piave basin of north-eastern Italy [25]. Taken together, these studies suggest that changes in Italian precipitation extremes are spatially and dynamically selective, and that their detection depends strongly on the spatial scale and on the type of descriptor adopted.

These approaches share a common limitation. They describe conditions at a single point or grid cell on a single day or, in the case of block maxima, the single most extreme value within a fixed period. They do not describe the event as a coherent physical object that forms, grows, moves, possibly splits or merges, and eventually decays. Two heatwaves that produce the same count of hot days at a weather station can have entirely different footprints and durations: one may be confined to a single valley for three days, whereas the other may cover the whole country for three weeks, with very different implications for the electricity grid, the health system and agriculture. Similarly, a short, intense, quasi-stationary convective cell and a slow-moving, multi-day organised system spanning several river basins pose very different hydrological and civil protection challenges, even when their peak intensity at a single rain gauge is comparable [26].

Object-based (event-based) methods address this gap by linking exceedance cells that are adjacent in space and time into a single spatiotemporal object, so that the life cycle of an event, i.e., its duration, evolving area, intensity and trajectory, can be measured directly. Studies adopting this paradigm agree that the spatial and temporal dimensions of an event, rather than its local peak intensity, largely control its overall magnitude. For precipitation, White et al. [27] tracked events in satellite and reanalysis products and showed that event duration strongly controls the total rainfall delivered, while Feng et al. [28] and Munoz et al. [29] developed object-based catalogues and tracking algorithms for mesoscale convective systems and convective storm cells, respectively. For heat, Lo et al. [14] defined heatwaves through the daily magnitude function of Russo et al. [30] and linked exceedance cells in space and time; using global reanalysis data since 1979, they showed that the growth in heatwave severity is driven mainly by increases in affected area and duration rather than by local intensity alone. A similar conclusion was reached for the record-breaking 2021 Pacific Northwest heatwave, whose unprecedented severity was explained mostly by its areal and temporal dimensions rather than by its peak temperature [31]. However, these studies differ in how they summarise the event population. Precipitation studies tend to describe convective systems as a continuum of sizes and intensities [28,29], whereas heatwave studies report aggregate statistics of the whole catalogue, such as mean duration and mean area [14,31]. In neither case are the events classified objectively into a small number of recurring dynamical types. Where such types are used, as in the distinction between local, propagating and quasi-stationary convective systems familiar to operational forecasters, they are generally imposed by the analyst rather than derived from the data. Moreover, almost all existing applications treat a single hazard in isolation. To our knowledge, no study has applied a joint event-tracking and unsupervised classification framework to both extreme heat and extreme precipitation over Italy, even though the country combines strong climatic heterogeneity with some of the highest documented impacts from both hazards in Europe. Italian studies on precipitation extremes, including our previous work on rainfall trends and generalised extreme value modelling in central Italy [9,17,22–24], and on heat extremes [6,7,15,16], have so far remained within the point-based or block-maxima paradigm.

The aim of this study is to determine whether the dynamical composition of heatwaves and extreme precipitation events over Italy changed between 1991 and 2020, i.e., whether all types of extreme events changed in frequency in the same way or whether the changes were concentrated in specific event types. It should be stressed that the percentile thresholds adopted here are conventional and are used only to identify candidate extreme cells; the methodological contribution lies in the subsequent spatiotemporal characterisation and classification of the resulting events. To achieve this aim, four specific objectives were pursued: (i) to build independent event catalogues of Italian heatwaves and extreme precipitation by applying three-dimensional (space–time) connected-component labelling to thirty years of

hourly ERA5 reanalysis data (1991–2020, the current WMO climatological standard normal period); (ii) to describe each event through a common set of eight dynamical features; (iii) to identify recurring event archetypes in each hazard with an unsupervised K-means algorithm, with the number of clusters selected through silhouette analysis rather than imposed a priori; and (iv) to test whether the annual frequency of each archetype changed over the study period, both nationally and at the grid-cell level. The main contributions of this work are as follows:

- A data-driven, unsupervised dynamical taxonomy of extreme events is proposed for Italy, in which archetypes are derived directly from event-scale features rather than defined a priori.
- The same object-based and unsupervised framework is applied to both extreme heat and extreme precipitation, allowing a direct comparison of changes in the dynamical composition of two distinct hazards over the same domain and period.
- The study shows that the increase in the frequency of extreme events over Italy since 1991 has not been uniform across event types but has been concentrated in the rarest, most persistent and most extensive archetype of each hazard, a pattern that is not readily apparent from conventional point-based indices.
- The framework relies entirely on freely available global reanalysis data and open-source software and is therefore potentially transferable to other regions with comparable climatic heterogeneity.

2. Materials and Methods

2.1. Study Area and Data

The study domain covers continental Italy, Sicily, Sardinia and the surrounding Tyrrhenian, Ionian and Adriatic waters, between 35.0 and 47.5 degrees north and between 6.0 and 19.0 degrees east (Figure 1a). The domain includes the Alpine arc in the north, the Apennine chain running the length of the peninsula, the Po valley, and the islands of Sicily and Sardinia, and therefore spans the full range of climatic and orographic settings found in Italy [4,5]. The study used the fifth-generation atmospheric reanalysis of the European Centre for Medium-Range Weather Forecasts, ERA5 [32]. Total precipitation and two-metre air temperature were extracted at native hourly temporal resolution and 0.25-degree spatial resolution, corresponding to approximately 28 kilometres in the north–south direction, for the period 1 January 1991 to 31 December 2020. This thirty-year window was chosen to match the current WMO climatological standard normal period, ensuring direct comparability with official climatological reporting [33]. Complementary satellite-based precipitation climatologies for Italy, derived independently from the IMERG mission, are also available and broadly consistent with the ERA5 seasonal precipitation distribution used here [34]. The domain contains 51 by 53 grid cells. Hourly precipitation was aggregated into daily totals. Hourly temperature was aggregated into daily maximum, minimum and mean values. The completeness of every one of the 10958 days in the record was verified for both variables before further analysis. For precipitation, the five days at the boundaries between source files (31 December 2000, 1 January 2001, 31 December 2010, 1 January 2011 and 31 December 2020) were excluded from event identification, i.e., 0.05% of the record.

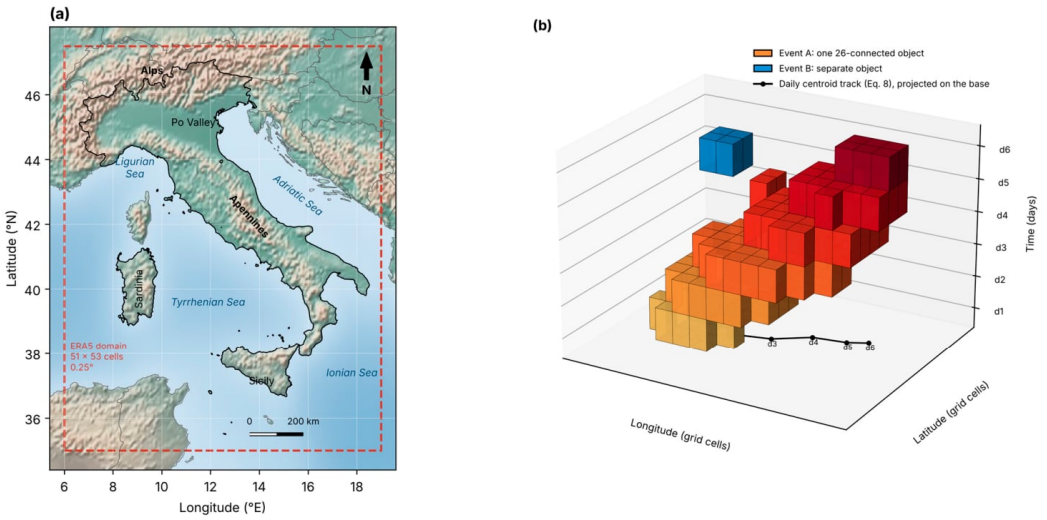

Figure 1. (**a**) Study area and analysis domain (dashed red box, 35.0–47.5° N, 6.0–19.0° E; 51 × 53 ERA5 grid cells at 0.25°), with the main orographic and geographical features, scale bar and north arrow; background shaded relief and boundaries from Natural Earth. (**b**) Schematic, synthetic illustration of the event-tracking framework: exceedance cells (cubes) that are adjacent in longitude, latitude or time, including diagonal adjacency (26-connectivity), are merged into a single three-dimensional object (event A; colours from light to dark indicate successive days), whereas a non-adjacent group of exceedance cells forms a separate object (event B). The black line shows the daily centroid (Equation (8)), projected onto the base, from which propagation speed and stationarity are computed (Equations (9) and (10)).

2.2. Identification of Extreme Events

For temperature, the calendar-day percentile approach of the Heat Wave Magnitude Index framework was adopted [13,14,30]. For every grid cell x and every calendar day d, a threshold was computed as the 90th percentile of daily maximum temperature within a 31-day window centred on d (i.e., from d − 15 to d + 15), pooling all thirty years of data (30 × 31 = 930 values per grid cell and calendar day). The window is circular, i.e., the days of the year are treated cyclically, so that the window wraps around the end of the calendar year: for example, the window for 1 January includes 17–31 December, and that for 31 December includes 1–15 January. This avoids truncated samples at the beginning and end of the year. The threshold is therefore

$$T_{thr}(x,d) = P_{90}(T_{max}(x,d')) \quad (1)$$

where d′ denotes the days of the window centred on d. A grid cell on a given day was flagged as an exceedance cell when its observed daily maximum temperature exceeded the local threshold. The corresponding exceedance magnitude, used later as an intensity measure, was defined following, in simplified form, the daily magnitude logic of Russo et al. [13,30] as

$$M(x,t) = T_{max}(x,t) - T_{thr}(x,d(t)) \quad (2)$$

for exceedance days, and zero otherwise, so that M quantifies only the positive departure above the local climatological threshold.

The thresholds were computed over the whole 1991–2020 period, which coincides with the WMO climatological standard normal adopted throughout this study [33]. A single, fixed base period ensures that changes in exceedance frequency are measured against a common climatological reference, and using the entire record as base period avoids the artificial discontinuity in exceedance rates between in-base and out-of-base years that affects percentile-based indices when the base period covers only part of the record. However,

because daily maximum temperature increased during 1991–2020, a threshold derived from the full record lies, by construction, above the climate of the earliest years and below that of the most recent ones. Part of the increase in heatwave occurrence detected in this study may therefore reflect the shift of the mean temperature relative to a fixed threshold, which tends to make events longer and more extensive, rather than changes in atmospheric dynamics alone. This behaviour is inherent to fixed-baseline definitions and is consistent with the heatwave-tracking literature [14,31], but it implies that the trends reported here should be interpreted as changes relative to the 1991–2020 climate. Separating the contribution of mean warming from that of changes in variability would require detrended or moving-baseline thresholds, as discussed among the limitations in Section 4.

For precipitation, a fixed, cell-specific threshold was used, defined as the 95th percentile of daily totals on wet days, a wet day being a day with at least 1 mm of precipitation, as in the ETCCDI very-wet-day index [12],

$$P_{thr}(x) = P_{95}(P(x,t)) \quad (3)$$

with the corresponding exceedance magnitude M(x,t) = P(x,t) − P_thr(x) for days exceeding the threshold. The choice of a fixed, non-seasonal threshold for precipitation, as opposed to a calendar-day-varying threshold for temperature, reflects established practice in the respective literature: seasonal exceedance is central to heatwave definition [13], whereas extreme precipitation in the Mediterranean, while more frequent in autumn, occurs throughout the year with a less sharply peaked seasonal cycle in its most extreme tail [19,21]. Exceedance cells were linked into three-dimensional objects using connected-component labelling [35] with 26-connectivity, that is, two exceedance cells (x1,t1) and (x2,t2) belong to the same object if they are adjacent in any combination of the two spatial and one temporal dimension, including diagonal adjacency (Figure 1b). This is the same logic used in previous object-based tracking studies of precipitation and heat extremes [14,27,28]. Each resulting object O is therefore a set of exceedance cells with a well-defined first day, last day and evolving spatial footprint. Heatwave objects lasting less than three days from their first to their last day were discarded, in analogy with the standard minimum heatwave duration criterion [13,14]; unlike in the HWMId, this criterion is applied to the object as a whole, so that individual grid cells within a retained object may exceed the threshold on fewer than three consecutive days. Precipitation objects consisting of a single cell on a single day were discarded as numerical noise; objects spanning at least two cell-days, including genuinely brief, localised two-cell bursts, were retained.

2.3. Event Feature Extraction

For every retained object O, eight descriptors were computed to characterise its dynamical behaviour rather than only its peak intensity. Grid-cell area was computed with the latitude-dependent correction for a regular latitude–longitude grid on a sphere [36],

$$A(x) = R^2 \Delta\varphi \Delta\lambda cos(\varphi(x)) \quad (4)$$

where R is the Earth radius, φ is latitude, λ is longitude, and Δφ and Δλ are the grid spacing in radians. Duration, in days, was defined as in previous event-based studies [14,27],

$$D(O) = t_{last}(O) - t_{first}(O) + 1 \quad (5)$$

Peak area, in square kilometres, was defined as the largest single-day footprint of the object [14],

$$A_{peak}(O) = \max_t \sum_{x \in O(t)} A(x) \quad (6)$$

In practice, the peak area of each object was approximated as the largest daily number of member cells multiplied by the area of a single grid cell (Equation (4)) evaluated at a reference latitude within the domain, rather than as the sum of the latitude-dependent areas of the individual cells in Equation (6). Compared with the exact form, this approximation underestimates peak area by about 7% on average (5th and 95th percentiles of the ratio between exact and approximate values: 0.99 and 1.20). Repeating the classification with the exact areas changed the archetype of 28 of the 1767 heatwave events (1.6%) and 22 of the 10,925 precipitation events (0.2%), and did not change the statistical significance of any of the archetype trends (Table S2, Supplementary Materials).

Mean and maximum intensity were computed over every member cell and day of the object using the exceedance magnitude M defined in Equations (2) and (3), and total volume was defined as the sum of M over the object, representing the cumulative severity of the event [14,27],

$$V(O) = \sum_{(x,t)\in O} M(x,t) \tag{7}$$

Following centroid-based storm-tracking methods [37], the spatial centroid of the object on day t was computed as the mean position of its N(t) member cells $x \in O(t)$, with the sums in Equation (8) running over these cells,

$$c(t) = \frac{\sum x}{\sum 1} \tag{8}$$

Propagation speed, in grid cells per day, was defined as the total path length travelled by the centroid, i.e., the sum of its day-to-day displacements, divided by the event duration [29,37],

$$S(O) = D(O)^{-1} \sum_t \|c(t+1) - c(t)\| \tag{9}$$

Spatial stationarity was defined as the ratio between the net displacement of the centroid over the whole event and the total path length travelled, analogous to the straightness index used in movement analysis [38],

$$St(O) = \frac{\left\|c(t_{last}) - c\left(t_{first}\right)\right\|}{\sum_t \|c(t+1) - c(t)\|} \tag{10}$$

which approaches one for an object that moves in a straight line without backtracking and approaches zero for an object that remains in place, oscillates, or expands in multiple directions without net translation. Finally, fragmentation was defined as the largest number of spatially disjoint, two-dimensionally connected sub-cores present within the object on any single day, capturing whether the event behaves as a single coherent system or as several simultaneously active, later merging or splitting, cores. For objects present on a single day, for which no displacement can be computed, propagation speed was set to zero and spatial stationarity to one by convention.

2.4. Unsupervised Classification

All eight features, duration, peak area, mean intensity, maximum intensity, total volume, propagation speed, stationarity and fragmentation, were standardised to zero mean and unit variance prior to clustering. K-means clustering [39] partitions n observations into k clusters by minimising the within-cluster sum of squared distances to each cluster centroid,

$$J = \sum_{i=1}^{k} \sum_{x\in C_i} \|x - \mu_i\|^2 \tag{11}$$

where C_i is the set of events assigned to cluster i and μ_i is its centroid in standardised feature space. The algorithm was run independently for the heatwave event set and for the extreme

precipitation event set, using ten random initialisations for each candidate value of k in the silhouette analysis and twenty for the final solution, with a fixed random seed to ensure reproducibility. The number of clusters was selected objectively using the mean silhouette coefficient [40], which for a given clustering compares, for every observation i, the mean within-cluster distance a(i) with the mean distance to the nearest other cluster b(i),

$$s(i) = \frac{b(i) - a(i)}{max\{a(i), b(i)\}} \quad (12)$$

with the mean silhouette score, averaged over all events, evaluated for k between two and eight (Figure S1, Supplementary Materials). For the precipitation catalogue, the silhouette score was computed on a random subsample of 4000 events for computational efficiency; for the final solution, the score computed on the full catalogue was virtually identical (0.66). For both hazards, the mean silhouette score was highest for k = 2 and, among solutions with at least three clusters, for k = 3. The two-cluster solutions only separate shorter and smaller events from longer and larger ones, and merge the rarest, most persistent and most extensive events with part of an intermediate group (for heatwaves, the 183 persistent nationwide heatwaves with 111 regional multi-day heatwaves; for precipitation, the 224 organised propagating systems with 668 persistent quasi-stationary systems). The three-cluster solution was therefore retained as the most parsimonious partition that isolates these rare events as a distinct class, and the sensitivity of the trend results to this choice was assessed by repeating the trend analysis for k = 2 and k = 4 (Table S1, Supplementary Materials). Following Kaufman and Rousseeuw [41], mean silhouette values between 0.26 and 0.50 were interpreted as indicating a weak structure, values between 0.51 and 0.70 a reasonable structure and values above 0.70 a strong structure. Each cluster was then interpreted physically using the mean of its members in the original, unstandardised feature units. Finally, the relative contribution of each feature to cluster separation was quantified by the ratio of the between-cluster variance to the total variance of the standardised feature (η^2, equivalent to the coefficient of determination of a one-way analysis of variance with the cluster label as factor). Values of η^2 close to one indicate features that differ strongly between archetypes, whereas values close to zero indicate features that contribute little to the partition.

2.5. Trend Analysis

For each archetype, the annual number of events was computed for every year of the record. Monotonic trends were tested with the non-parametric Mann–Kendall test [42,43], which for a time series x_1, ..., x_n computes the statistic

$$S = \sum_{i<j} \text{sign}(x_j - x_i) \quad (13)$$

with S approximately normally distributed for the sample sizes used here, variance

$$Var(S) = \frac{n(n-1)(2n+5)}{18} \quad (14)$$

and standardised test statistic

$$Z = \frac{S - sign(S)}{\sqrt{Var(S)}} \quad (15)$$

A trend was considered statistically significant at the conventional $\alpha = 0.05$ level when the two-sided *p* value associated with Z was below 0.05. The magnitude of significant trends was quantified with the Sen's slope estimator [44], the median of all pairwise slopes,

$$\beta = median \frac{x_j - x_i}{j - i}, i < j \quad (16)$$

which is robust to outliers and does not assume normally distributed residuals, a desirable property for short, count-based climate time series. The Mann–Kendall test and Sen's slope estimator are standard, widely validated choices in hydroclimatic trend detection and have been used extensively in previous Italian precipitation and temperature trend studies, including our own [9,17,22–24]. The same procedure was applied at the grid-cell level to the most extreme archetype of each hazard, using the annual count of member cell-days at each pixel, in order to map where its increase is concentrated. All analyses were performed in Python 3.12, using scikit-learn [45] for clustering and silhouette analysis, and SciPy [46] for statistical testing and for the connected-component labelling routine (scipy.ndimage) used for event identification. The Mann–Kendall test was implemented as Kendall's rank correlation between the annual counts and time (scipy.stats.kendalltau, which includes a correction for ties), and Sen's slope with scipy.stats.theilslopes. Because 2703 local tests were performed and neighbouring grid cells are spatially correlated, the proportion of locally significant cells was compared with the approximately 5% expected by chance at $\alpha = 0.05$, and local results were interpreted with caution [47].

3. Results

The event-based classification reveals an asymmetry between event types that is not readily apparent from conventional point-based analyses. For both heatwaves and extreme precipitation, three dynamical archetypes were retained (Section 2.4), and in both hazards the rarest and most extensive archetype, rather than the more common extremes, accounts for all of the statistically significant changes in frequency detected between 1991 and 2020. The following subsections present, for each hazard, the taxonomy of the archetypes and their temporal evolution.

3.1. Heatwaves

3.1.1. A Three-Archetype Taxonomy of Italian Heatwaves

The event-tracking procedure identified 1767 heatwave events over Italy between 1991 and 2020, each lasting at least three days. The three-cluster solution retained (Section 2.4; Figure S1) has a mean silhouette score of 0.32. This value falls within the range that Kaufman and Rousseeuw [41] associate with a weak structure: the three archetypes are distinguishable and physically interpretable, but they partly overlap, particularly at the transition between brief localised spikes and regional multi-day heatwaves. They should therefore be regarded as typical modes of a partly continuous population of events rather than as sharply separated classes. Table 1 summarises the mean values of all eight clustering features for each archetype, together with the contribution of each feature to cluster separation (η^2).

Table 1. Mean characteristics of the three heatwave archetypes identified by unsupervised clustering, Italy, 1991–2020, for all eight clustering features. η^2 is the ratio of between-cluster to total variance of each standardised feature.

Feature	Brief Localised Spikes	Regional Multi-Day Heatwaves	Persistent Nationwide Heatwaves	η^2
Number of events	994	590	183	–
Duration (days)	3.6	5.5	15.5	0.61
Peak area (km^2)	30,266	188,994	796,490	0.75
Mean intensity (°C)	0.50	1.09	1.17	0.50
Maximum intensity (°C)	1.7	4.4	6.8	0.67

Table 1. *Cont.*

Feature	Brief Localised Spikes	Regional Multi-Day Heatwaves	Persistent Nationwide Heatwaves	η^2
Total volume (°C·cell-days)	59	964	10,458	0.54
Propagation speed (grid cells day^{-1})	2.07	5.37	7.17	0.50
Spatial stationarity (-)	0.64	0.57	0.31	0.10
Fragmentation (number of cores)	1.9	4.5	12.0	0.66

Peak area was approximated as described in Section 2.3. Spatial stationarity is the ratio between net and total centroid displacement (Equation (10)).

Brief localised spikes are the most numerous archetype, but they affect small areas and dissipate quickly, consistent with short-lived heat excursions confined to a single sub-region. Regional multi-day heatwaves cover roughly a quarter of the domain at their peak and last around one working week. Persistent nationwide heatwaves are rare, with only 183 events recorded over thirty years, but they show the highest values of duration, peak area, maximum intensity and fragmentation. On average, they last more than two weeks, cover nearly the entire domain at their peak, reach a maximum intensity four times higher than that of brief localised spikes and contain about twelve simultaneously active hot cores. This suggests a distinct large-scale configuration rather than simply a longer version of an ordinary heatwave. The archetypes also differ in the remaining features (Table 1). Mean intensity is about twice as high in regional multi-day and persistent nationwide heatwaves (1.1 and 1.2 °C) as in brief localised spikes (0.5 °C), while total volume increases by more than two orders of magnitude from brief localised spikes to persistent nationwide heatwaves, reflecting the combined growth of duration, extent and intensity. Propagation speed increases (from 2.1 to 7.2 grid cells per day) and spatial stationarity decreases (from 0.64 to 0.31) from brief localised spikes to persistent nationwide heatwaves; for the latter, the low stationarity indicates centroid displacements without a consistent net direction, as expected for events that expand, contract and fragment across the whole domain rather than translate. Peak area ($\eta^2 = 0.75$), maximum intensity (0.67) and fragmentation (0.66) contribute most to the separation of the heatwave archetypes, whereas spatial stationarity contributes little (0.10). Figure 2 shows the spatial density of each archetype, expressed in cell-days, i.e., the number of days on which each grid cell belonged to an event of that archetype over 1991–2020 (an event lasting 3 days and covering 10 cells contributes 30 cell-days). Brief localised spikes (Figure 2a) produce low, diffuse values over the whole domain without a dominant area, consistent with small, scattered events. Persistent nationwide heatwaves (Figure 2b) produce high values almost everywhere, confirming that this archetype affects the whole country rather than a specific region, although values are somewhat higher in central and southern Italy and in inland areas than along the coast. Regional multi-day heatwaves (Figure 2c) show an intermediate pattern with clearer geographical gradients, with higher values in northern Italy, Calabria, Sicily, the Adriatic side of the Apennines and the Apennine foothills.

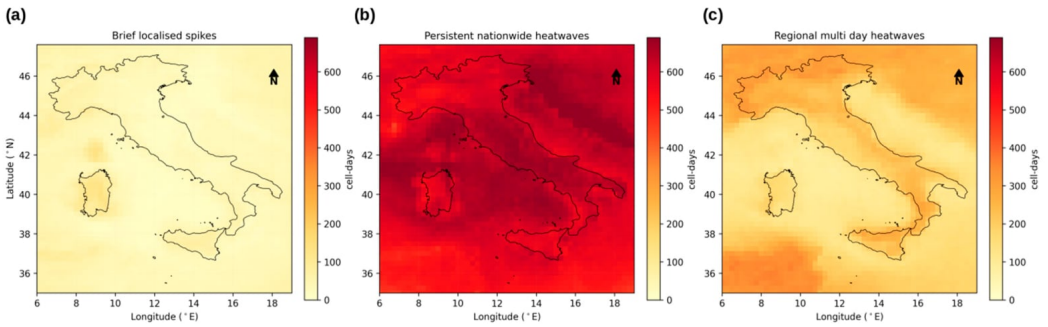

Figure 2. Spatial density, in cell-days, of each heatwave archetype over the domain, 1991–2020: (**a**) brief localised spikes; (**b**) persistent nationwide heatwaves; (**c**) regional multi-day heatwaves. North arrow and coordinate grid are shown on each panel.

Figure 3 shows each heatwave event in the space defined by duration and peak area, which provides a compact dynamical fingerprint of Italian heatwaves.

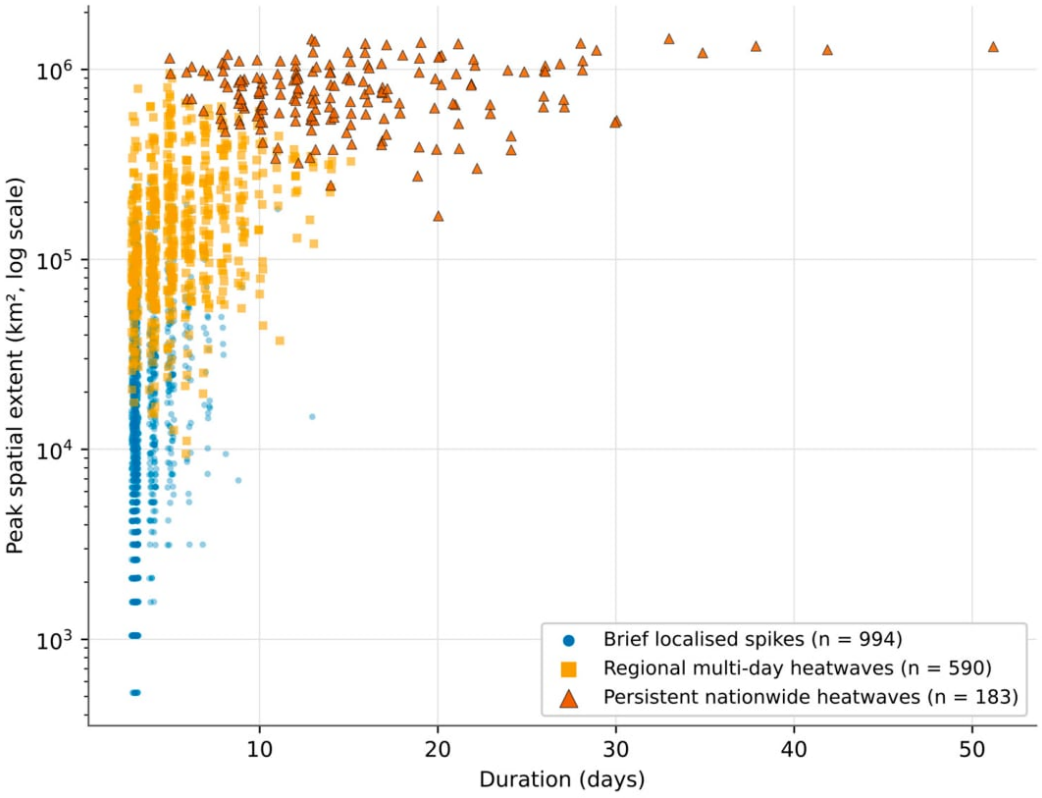

Figure 3. Dynamical fingerprint of Italian heatwave events. Each point is one event, positioned by its duration (x-axis, days) and peak spatial extent (y-axis, km^2, logarithmic scale) and coloured by its assigned archetype.

The three archetypes occupy distinct but partly overlapping regions of this space. Brief localised spikes are confined to short durations, mostly between three and seven days, and to peak areas mostly below about 10^5 km^2, with peak area tending to increase with duration. Regional multi-day heatwaves have similar or slightly longer durations but substantially larger peak areas, mostly between about 3×10^4 and 10^6 km^2; their overlap with brief localised spikes at short durations and intermediate areas is consistent with the modest silhouette score obtained for heatwaves. Persistent nationwide heatwaves are more clearly separated from the other two archetypes: they last from about five days to more than seven weeks, while their peak area ranges mostly between about 3×10^5 km^2 and the total area

of the domain (about 1.6×10^6 km^2). For this archetype, peak area therefore saturates at the size of the domain, and the variability among events is expressed mainly by duration. Overall, peak area increases with duration across the heatwave population, and the three archetypes correspond to different combinations of persistence and spatial extent, with a sharper boundary for the persistent nationwide archetype than between the two more frequent archetypes.

3.1.2. Temporal Evolution of the Heatwave Archetypes

The three archetypes followed different trajectories over 1991–2020. Persistent nationwide heatwaves increased from about three events per year in the early 1990s to about ten events per year by 2020, a more than threefold rise, with a Kendall's τ of 0.69 ($p < 0.0001$), the strongest trend detected in this analysis. Brief localised spikes and regional multi-day heatwaves showed positive Sen's slopes but no statistically significant monotonic trend over the full period ($p = 0.21$ and $p = 0.61$, respectively). In other words, the annual frequency of the more common heatwave types did not change significantly between 1991 and 2020, whereas the nationwide, multi-week archetype became several times more frequent. Table 2 reports the trend statistics.

Figure 4 shows the annual number of heatwave events per archetype, 1991–2020. Solid lines connect the yearly counts of each archetype, and dashed lines of matching colour show the corresponding linear trend. Only the persistent nationwide archetype shows a statistically significant upward trend, whereas the trend lines of the other two archetypes remain comparatively flat.

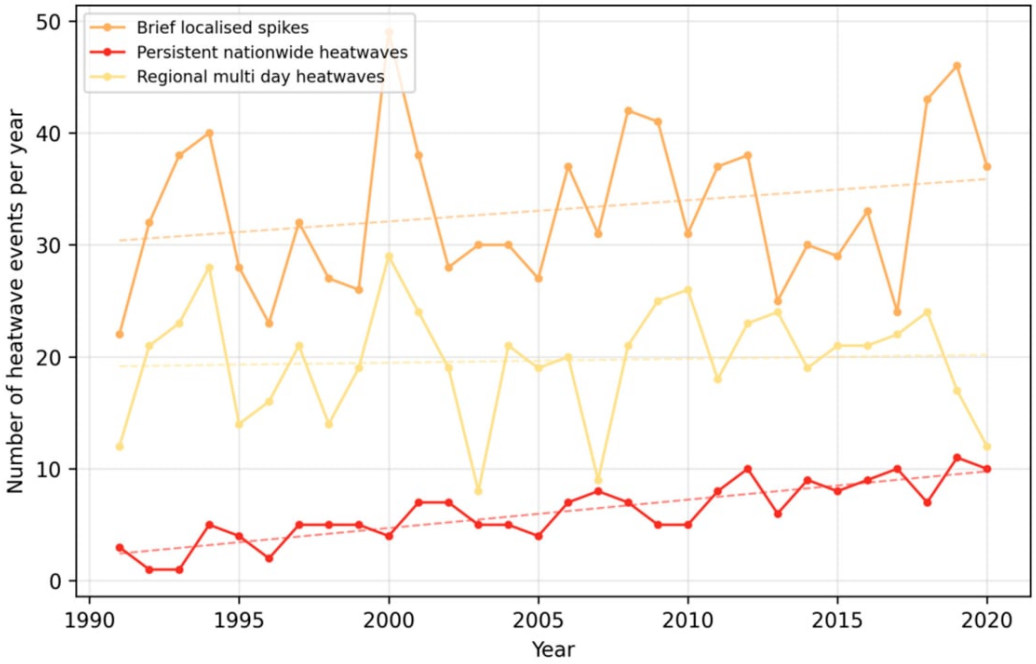

Figure 4. Annual number of heatwave events per archetype, 1991–2020, with linear trend lines.

The spatial pattern of this increase, shown in Figure 5, is close to uniform across the country, consistent with the nationwide character of this archetype. Of the 2703 grid cells, 2634 (97%) show a statistically significant ($p < 0.05$) increasing trend in the local frequency of persistent nationwide heatwave days, far more than the approximately 5% that would be expected by chance alone [47]. The temporal result is robust to the number of clusters: with k = 2, only the class containing the persistent nationwide heatwaves shows a significant increase ($\tau = 0.58$, $p < 0.0001$), and with k = 4 significant increases are found only for the

two classes with the longest durations and largest extents ($\tau = 0.35$, $p = 0.009$ and $\tau = 0.59$, $p < 0.0001$; Table S1).

Table 2. Mann–Kendall trend statistics for the annual frequency of each heatwave archetype, 1991–2020.

Archetype	Kendall's τ	*p* Value	Sen's Slope, Events per Decade
Brief localised spikes	0.16	0.21	2.2
Regional multi-day heatwaves	0.07	0.61	0.4
Persistent nationwide heatwaves	**0.69**	**<0.0001**	**2.5**

Values in bold indicate statistically significant trends at $p < 0.05$ (two-sided Mann–Kendall test).

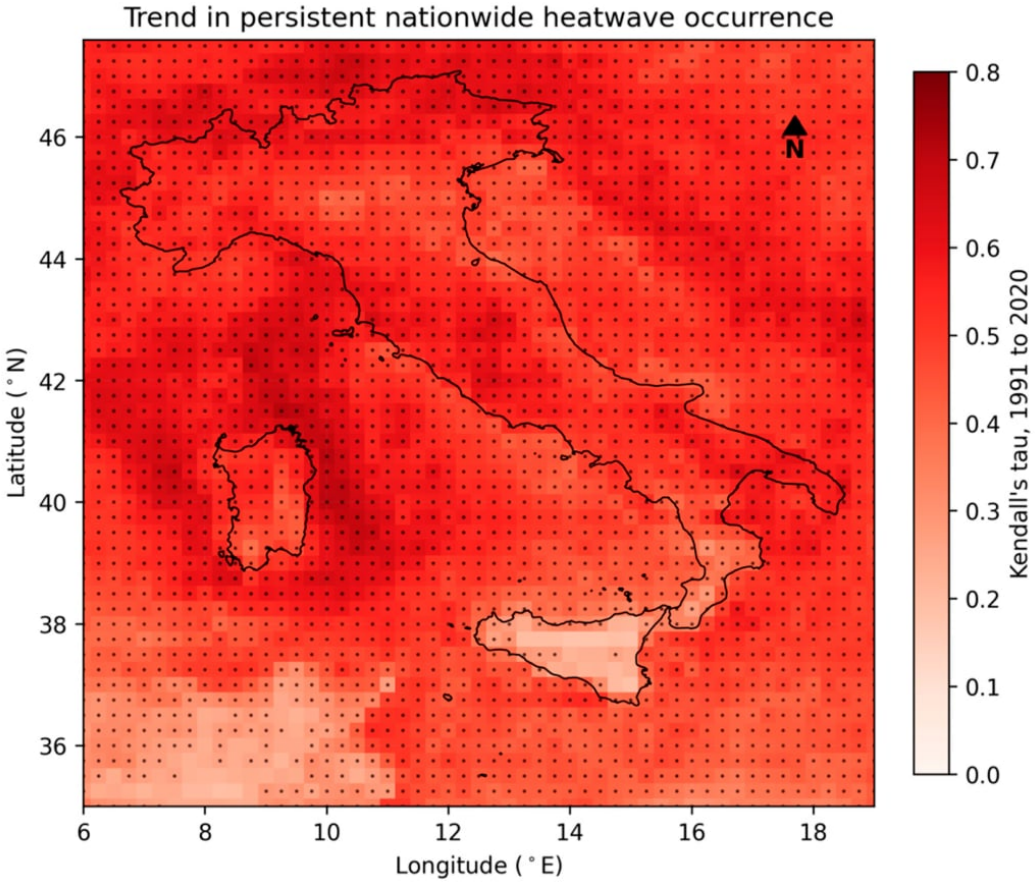

Figure 5. Local Kendall's τ for the trend in persistent nationwide heatwave occurrence, 1991–2020. Dots mark grid cells with $p < 0.05$. North arrow and coordinate grid are shown.

3.2. Extreme Precipitation

3.2.1. A Three-Archetype Taxonomy of Italian Extreme Precipitation

The event-tracking procedure identified 10,925 extreme precipitation events between 1991 and 2020. The mean silhouette score of the three-cluster solution was 0.66 (Figure S1), which corresponds to a reasonable cluster structure according to Kaufman and Rousseeuw [41] and indicates a clearer separation than for heatwaves. Table 3 summarises the mean values of all eight clustering features for each archetype, together with the contribution of each feature to cluster separation (η^2).

Table 3. Mean characteristics of the three extreme precipitation archetypes identified by unsupervised clustering, Italy, 1991–2020, for all eight clustering features. η^2 is the ratio of between-cluster to total variance of each standardised feature.

Feature	Local Bursts	Persistent Quasi-Stationary Systems	Organised Propagating Systems	η^2
Number of events	9284	1417	224	-
Duration (days)	1.1	2.4	4.2	0.60
Peak area (km^2)	6672	47,195	171,890	0.66
Mean intensity (mm)	3.64	10.21	13.26	0.42
Maximum intensity (mm)	8.2	37.4	71.6	0.63
Total volume (mm·cell-days)	69	1249	7869	0.66
Propagation speed (grid cells day^{-1})	0.13	2.88	7.08	0.64
Spatial stationarity (-)	1.00	0.87	0.65	0.29
Fragmentation (number of cores)	1.0	1.6	3.7	0.55

Peak area was approximated as described in Section 2.3. Spatial stationarity is the ratio between net and total centroid displacement (Equation (10)); for single-day events it is set to one by convention, which explains the value for local bursts.

Local bursts dominate the catalogue by event count, with 9284 events, compared with 1417 persistent quasi-stationary systems and 224 organised propagating systems. They are short-lived (1.1 days on average), spatially limited at peak (6672 km^2) and characterised by relatively low maximum intensity (8.2 mm) and minimal fragmentation (1.0), consistent with isolated or weakly organised precipitation bursts. Persistent quasi-stationary systems are less frequent but longer-lived, with a mean duration of 2.4 days, a substantially larger peak area (47,195 km^2) and a higher maximum intensity (37.4 mm). Their low-to-moderate fragmentation is consistent with spatially coherent systems that remain relatively stationary, as reported for slow-moving precipitation systems over Liguria and the Adriatic side of the Apennines [10,11]. Organised propagating systems are the rarest archetype, comprising 224 events, or about 2% of the catalogue. They have the longest mean duration (4.2 days), the largest peak area (171,890 km^2), the highest maximum intensity (71.6 mm) and the greatest fragmentation (3.7), indicating larger and more spatially complex precipitation systems. Here, peak area refers to the maximum geographical extent of an individual event, rather than to the number of raster cells or the number of events assigned to an archetype. Mean intensity increases from 3.6 mm in local bursts to 10.2 mm in persistent quasi-stationary systems and 13.3 mm in organised propagating systems, and total volume increases by about two orders of magnitude across the three archetypes (Table 3). Propagation speed is close to zero for local bursts, most of which last a single day, and increases to 2.9 and 7.1 grid cells per day in persistent quasi-stationary and organised propagating systems, respectively, while spatial stationarity decreases from 0.87 to 0.65. The value of 1.00 for local bursts reflects the convention adopted for single-day events (Section 2.3) rather than straight-line motion. Total volume ($\eta^2 = 0.66$), peak area (0.66), propagation speed (0.64) and maximum intensity (0.63) contribute most to the separation of the precipitation archetypes, and spatial stationarity least (0.29).

Figure 6 shows the spatial density of each precipitation archetype, expressed as the cell-days accumulated over 1991–2020, i.e., how many times each grid cell was affected by an event of that type, weighted by its duration. Local bursts (Figure 6a) are most frequent

along the Alpine arc, particularly at its north-western end, and over the eastern Adriatic coast, consistent with isolated convective events favoured by orographic forcing. Organised propagating systems (Figure 6b) show a more widespread pattern, less concentrated in a single band, with relatively high values along the southern side of the Alps and across several corridors, including Liguria, the central Adriatic coast and Sicily. This is consistent with systems that move during their lifetime and therefore affect many cells along their path rather than remaining over a single area. Persistent quasi-stationary systems (Figure 6c) show the most pronounced pattern, with a very dark band along the northern side of the Alpine arc and high values over the eastern Adriatic coast. These systems remain over the same area for a long time and therefore accumulate many cell-days where they form, typically where the terrain blocks the moist airflow. Figure 7 shows the corresponding dynamical fingerprint in the duration–peak area space.

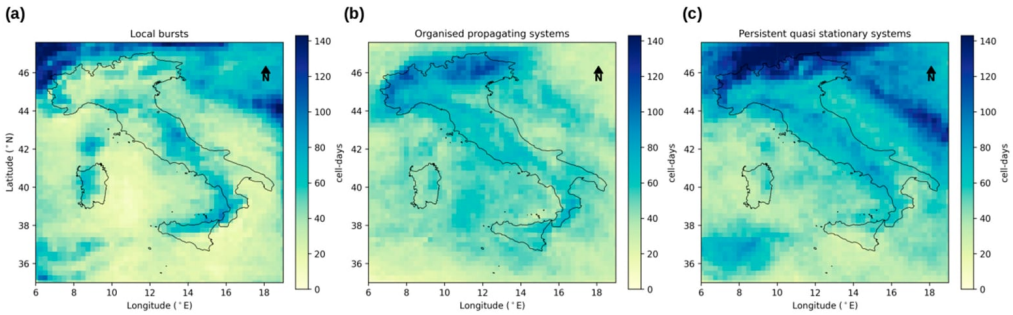

Figure 6. Spatial density, in cell-days, of each extreme precipitation archetype over the domain, 1991–2020: (**a**) local bursts; (**b**) organised propagating systems; (**c**) persistent quasi-stationary systems. North arrow and coordinate grid are shown on each panel.

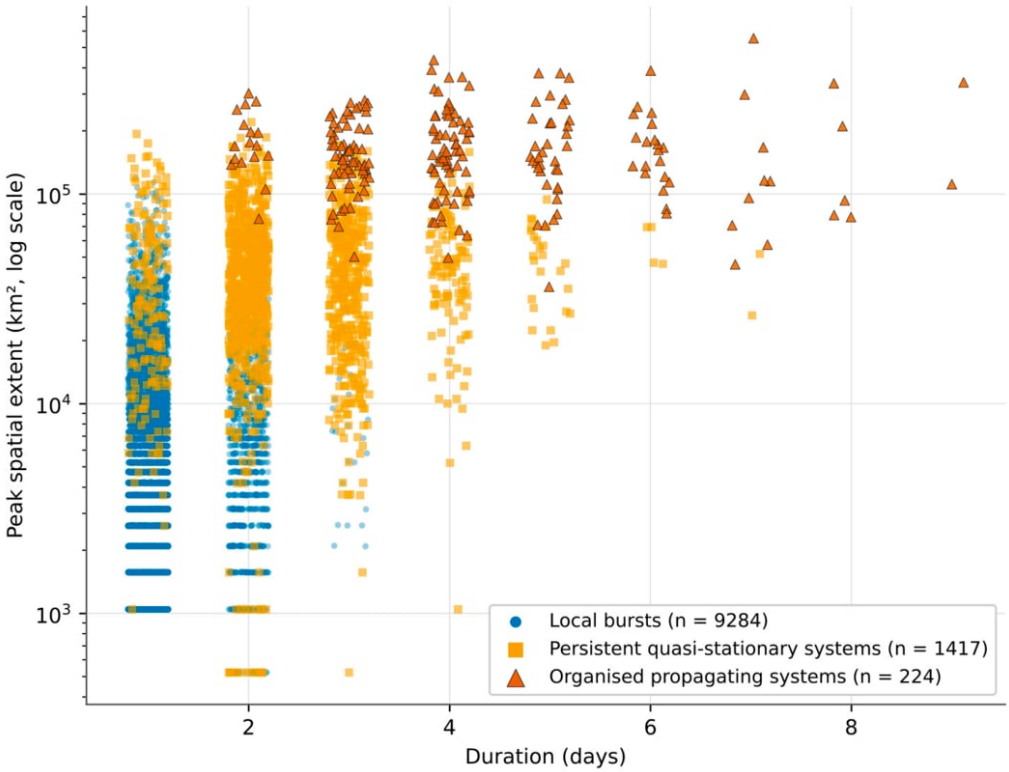

Figure 7. Dynamical fingerprint of Italian extreme precipitation events. Each point is one event, positioned by its duration (x-axis, days) and peak spatial extent (y-axis, km^2, logarithmic scale) and coloured by its assigned archetype.

The precipitation archetypes have a higher mean silhouette score than the heatwave archetypes (0.66 versus 0.32), but in this two-dimensional projection they still partly overlap, in particular local bursts and persistent quasi-stationary systems at durations of one to two days and peak areas between about 10^4 and 10^5 km^2. Local bursts, which number in the thousands, are concentrated at durations of one to two days and peak areas from about 10^3 to 10^5 km^2. Persistent quasi-stationary systems mostly last two to five days, with peak areas between about 10^4 and 2×10^5 km^2. Organised propagating systems occupy the upper part of the diagram, with durations from two to nine days and peak areas mostly above 10^5 km^2. In all archetypes, peak area tends to increase with duration, but, unlike the largest heatwaves, precipitation events remain well below the size of the domain; duration and peak area therefore jointly discriminate the archetypes, and the separation visible in this projection is complemented by the other features, notably maximum intensity and fragmentation (Table 3). The rarest archetype is thus also the most extreme in duration, peak area and maximum intensity.

3.2.2. Temporal Evolution of the Extreme Precipitation Archetypes

As for heatwaves, only the rarest precipitation archetype shows a statistically significant upward trend (Kendall's $\tau = 0.43$, $p = 0.0017$). Organised propagating systems nearly doubled in frequency, from about five to seven events per year in the early 1990s to about nine to eleven events per year by 2020. Local bursts showed a positive but non-significant trend ($p = 0.07$), and persistent quasi-stationary systems showed no significant trend ($p = 0.17$). The archetype with the highest maximum intensity, the largest peak area and the longest duration is therefore also the only one whose frequency increased significantly. Table 4 reports the trend statistics and Figure 8 shows the annual counts. The significant increase in organised propagating systems is robust to the number of clusters (k = 4: $\tau = 0.32$, $p = 0.017$ for the class of the longest and largest events; Table S1), but the borderline increase in the numerous short-lived events becomes significant in the alternative partitions (k = 2: $\tau = 0.27$, $p = 0.038$; k = 4: $\tau = 0.26$, $p = 0.045$). With k = 2, in which organised propagating systems are merged with part of the persistent quasi-stationary systems, the class of the longer and larger events shows no significant trend ($\tau = 0.13$, $p = 0.32$). For precipitation, the conclusion that the increase is confined to the rarest archetype therefore depends on the partition, and a weak increase in short-lived local events cannot be excluded.

The annual counts of local bursts and persistent quasi-stationary systems fluctuate considerably from year to year but show no statistically significant trend, whereas organised propagating systems, although far less numerous, show a statistically significant upward trend (Table 4). The increase in organised propagating systems is not uniform across the domain (Figure 9). Of the 2703 grid cells, 254 (about 9%) show a statistically significant ($p < 0.05$) increase in the annual number of cell-days affected by this archetype, and 3 a significant decrease. This proportion should be interpreted with caution, because about 5% of the cells would be expected to be significant by chance alone at this level and neighbouring cells are spatially correlated [47]; the signal is therefore more informative for its spatial coherence than for its areal extent. The significant cells form spatially coherent clusters over the Ligurian Sea and western Sardinia, over the central Apennines, mainly on their Adriatic side, and over Calabria and north-eastern Sicily, areas that the literature repeatedly associates with severe Mediterranean cyclones and flash floods [8–11]. This spatial coincidence shows that the increase in this archetype is concentrated in specific areas; establishing whether it is linked to changes in specific storm tracks would require a dedicated analysis of cyclone tracks, which was beyond the scope of this study.

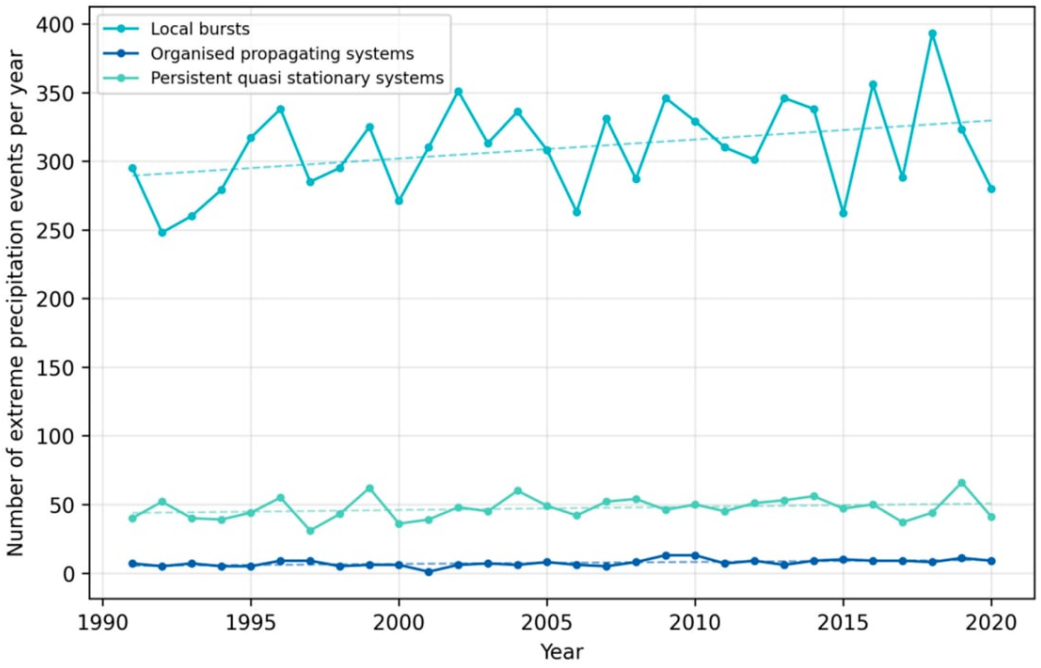

Figure 8. Annual number of extreme precipitation events per archetype, 1991–2020, with linear trend lines.

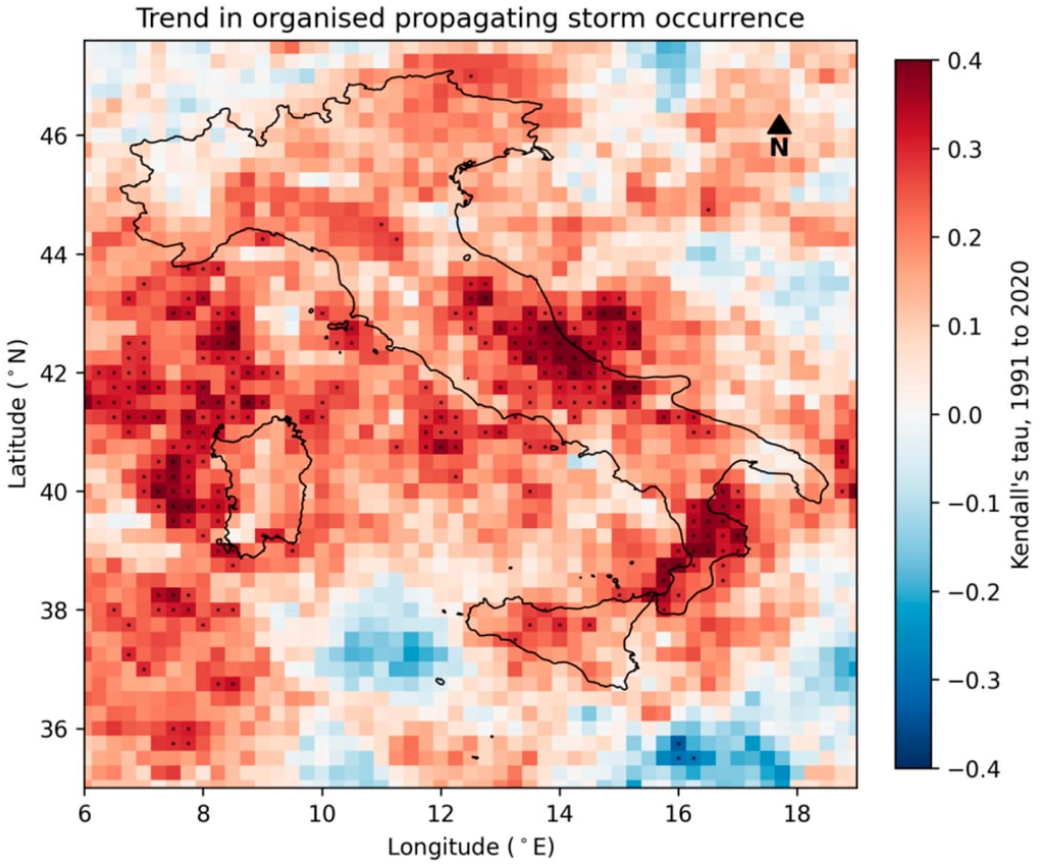

Figure 9. Local Kendall's τ for the trend in organised propagating storm occurrence, 1991–2020. Dots mark grid cells with $p < 0.05$. North arrow and coordinate grid are shown.

Table 4. Mann–Kendall trend statistics for the annual frequency of each precipitation archetype, 1991–2020.

Archetype	Kendall's τ	*p* Value	Sen's Slope, Events per Decade
Local bursts	0.24	0.07	16.0
Persistent quasi-stationary systems	0.18	0.17	2.8
Organised propagating systems	**0.43**	**0.0017**	**1.4**

Values in bold indicate statistically significant trends at $p < 0.05$ (two-sided Mann–Kendall test).

4. Discussion

The central finding of this study is consistent across two very different hazards. For both heat and precipitation extremes over Italy, the increase in event frequency between 1991 and 2020 was not uniform across event types: it was concentrated in the rarest, most persistent and most extensive dynamical archetype, while the more common archetypes showed no statistically significant change in frequency. Conventional analyses based on annual maxima, block-maxima extreme value fits or percentile counts can detect changes in extremes, but, because they pool all dynamical types together, they may not easily distinguish an increase driven by many small events from one driven by a few large and persistent events. The event-based classification adopted here makes this distinction explicit and therefore complements, rather than replaces, these established approaches.

For heatwaves, the results agree with the event-based tracking literature, which has shown at the global scale that increases in heatwave severity are driven mainly by growth in event size and duration rather than by a uniform rise in daily temperature everywhere [14,31]. The present results extend this picture to the national scale in Italy and show that the increase in the persistent nationwide archetype is remarkably homogeneous in space, affecting nearly the whole country. This homogeneity is compatible with a large-scale driver, such as a more frequent and more persistent subtropical ridge over the central Mediterranean, rather than with a purely local land-surface effect, although the atmospheric circulation was not analysed here and this interpretation remains to be tested. The results are also broadly consistent with recent national-scale assessments reporting a marked rise in extreme heat days and heatwave-related mortality risk across Italy over approximately the same period [6,7]. Compared with Lo et al. [14], who attributed severity growth jointly to area and duration without separating discrete regimes, the present classification indicates that, in terms of frequency, the significant increase occurred in only one identifiable archetype. Whether the same holds for other severity dimensions, such as the intensity or volume of individual events, was not tested and would require dedicated analyses. As discussed in Section 2.2, part of this increase may also reflect the shift of mean temperature relative to the fixed 1991–2020 threshold, which tends to make events longer and more extensive.

For precipitation, the comparison with recent international work reveals both agreement and differences. In agreement with White et al. [27], event duration appears central: the organised propagating archetype identified here lasts on average about four times longer than a local burst and also has a much larger peak area and maximum intensity (Table 3). Feng et al. [28] and Munoz et al. [29], in contrast, describe mesoscale convective systems and severe convective cells largely as a continuum of sizes and intensities, without reporting a comparably distinct, trend-bearing separation between a rare, organised class and a numerous, less organised one. The higher silhouette score obtained here for precipitation (0.66) than for heatwaves (0.32) suggests that Italian extreme precipitation

events, as resolved by ERA5 at daily resolution, may be more regime-like than heatwaves. However, differences in data, resolution and tracking criteria among studies prevent a direct comparison, and this finding invites further comparative work in other Mediterranean and mid-latitude domains.

Unlike the heatwave signal, the increase in organised propagating systems is spatially concentrated. Significant local trends cluster over the Ligurian Sea and western Sardinia, the central Apennines and Calabria–north-eastern Sicily, areas that have been repeatedly affected by severe floods in past decades, including the 2022 Marche–Umbria event and recurrent Ligurian flash floods [8–10]. A national average trend would therefore understate the change occurring in these areas, in line with recent findings that national-scale analyses based on coarse-resolution datasets can obscure locally concentrated intensification driven by mesoscale orographic and coastal effects [18,20,21]. The proportion of the domain with a significant local trend (about 9%) is broadly consistent with regional studies reporting that a minority of areas, of the order of 10–15%, show significant increases in the frequency or intensity of the heaviest daily rainfall across northern and central Italy [21]. The present analysis adds that, in the ERA5 record, this increase is associated specifically with the rarest, most organised event type rather than with extreme rainfall in general. However, the spatial coincidence between significant cells and areas frequently affected by Mediterranean cyclones does not by itself establish a cyclogenesis mechanism; linking archetype occurrence to cyclone tracks and to the large-scale circulation is a necessary next step.

This dynamical perspective may also help to interpret the results of non-stationary extreme value analyses. Recent applications of the generalised extreme value distribution to central Italian rainfall have found that return levels estimated from shorter, more recent sub-periods systematically exceed those estimated from the full historical record, and that adding a single exceptional year can substantially shift the fitted distribution [9,22]. One possible interpretation, which should be regarded as a hypothesis, is that block-maxima series are increasingly populated by events belonging to the rarest, most organised archetype, rather than by more intense draws from an unchanged distribution. Testing this hypothesis would require linking the archetype membership of each event to the composition of annual maxima series, which was not done here. The hypothesis is nevertheless consistent with recent evidence of non-stationary behaviour at sub-daily resolution in the Piave basin of north-eastern Italy [25] and with calls in the literature for climate risk assessment to move beyond single-distribution, stationary assumptions [23,24].

From a risk perspective, the archetypes whose frequency is increasing are, in both hazards, those with the most extreme physical characteristics, namely the longest duration, the largest extent and the highest maximum intensity. Such characteristics are generally associated with a high impact potential. Persistent nationwide heatwaves may place simultaneous stress on the population and on the electricity and health care systems across the whole country, a configuration relevant to the heatwave health warning systems already operating in Italian cities [6]. Organised propagating systems combine high rainfall intensity with large affected areas and multi-day duration, which are typical ingredients of the major flood and landslide disasters documented for Marche, Umbria and Liguria [8–10]. However, impacts, exposure and vulnerability were not quantified in this study, and the link between archetypes and damage remains to be demonstrated. With this caveat, the results suggest that these archetypes, and the areas in which they are becoming more frequent, deserve particular attention in adaptation planning and in the design of early warning systems.

Several limitations should be considered. First, ERA5 has a native resolution of 0.25 degrees, which smooths the most localised convective extremes and may underestimate peak rainfall intensity compared with convection-permitting models or dense rain gauge networks [48,49]. Second, the thresholds, a fixed high percentile for precipitation and a

calendar-day percentile for temperature, are standard and defensible choices, consistent with the previous Italian and international literature [9,13,17,50], but different thresholds, base periods or connectivity rules could shift the balance between archetypes. In particular, thresholds computed on detrended data or on a moving baseline would help to separate the effect of mean warming from that of changes in variability (Section 2.2), and a systematic sensitivity analysis is therefore a natural next step. Third, the three-dimensional connectivity rule allows events to split and merge implicitly through shared labels, but it does not explicitly track the identity of individual sub-cores as dedicated storm-tracking algorithms do [29,37]; moreover, the peak area of the largest heatwaves is bounded by the size of the domain. Fourth, the heatwave clustering shows only weak-to-moderate separation (silhouette score 0.32), so the boundaries between heatwave archetypes, particularly between brief localised spikes and regional multi-day heatwaves, should be considered approximate. Fifth, grid-cell trends were tested individually; given the large number of tests and the spatial correlation between neighbouring cells, a formal field-significance assessment, for example based on the false discovery rate [47], would strengthen the interpretation of the local trend maps. Sixth, for precipitation, the trend results are partly sensitive to the number of clusters, since the borderline increase of local bursts becomes significant for k = 2 and k = 4 (Section 3.2.2). Finally, thirty years is a relatively short window for trend detection. Statistical significance over 1991–2020 does not by itself separate the forced climate change signal from multi-decadal internal variability [51], nor does it guarantee that the trends are robust to the choice of period. Extending the record backward with longer reanalysis products or homogenised station networks [15,16], and performing a formal attribution analysis, would be required to establish the causes of the observed changes. For these reasons, the results are best interpreted as a description of how the frequency of different event types changed over the most recent WMO climatological standard normal period, consistent with, but not in themselves proof of, a climate change signal.

5. Conclusions

This study developed an event-based framework that tracks heatwaves and extreme precipitation over Italy as three-dimensional objects and classifies them into archetypes through unsupervised clustering, without categories imposed in advance. Applied to ERA5 reanalysis data for 1991–2020, the method identified three heatwave archetypes (brief localised spikes, regional multi-day heatwaves and persistent nationwide heatwaves) and three precipitation archetypes (local bursts, persistent quasi-stationary systems and organised propagating systems), each with a physically interpretable dynamical signature. The precipitation archetypes are reasonably well separated (silhouette score 0.66), whereas the heatwave archetypes show weak-to-moderate separation (0.32) and partly overlap. The key result is that the frequency of extreme events did not change uniformly across event types. In both hazards, only the rarest archetype, characterised by the longest duration, the largest extent and the highest maximum intensity, showed a statistically significant increase in annual frequency, although for precipitation a weaker increase in local bursts ($p = 0.07$) becomes significant in alternative partitions. Persistent nationwide heatwaves rose from about three to about ten events per year (Kendall's $\tau = 0.69$, $p < 0.0001$), with significant local increases over 97% of the grid cells. Organised propagating systems nearly doubled in frequency ($\tau = 0.43$, $p = 0.0017$), but significant local increases were found in only 9% of the grid cells (254 of 2703), clustered over the Ligurian Sea and western Sardinia, the central Apennines and Calabria–north-eastern Sicily. These findings show that an event-based dynamical classification can reveal changes that are not readily apparent from conventional point-based indices, and that treating an event catalogue as a single population may obscure changes concentrated in specific event types. The trends refer to changes in

frequency over a thirty-year period and should not be attributed to anthropogenic climate change without a dedicated attribution analysis. Because it relies on open reanalysis data and open-source software, the framework is adaptable to other regions and datasets. Future work should test the sensitivity of the results to thresholds and base periods, extend the analysis to longer records and to convection-permitting simulations, and link the archetypes to atmospheric circulation and to observed impacts, in order to support adaptation and civil protection planning.

Supplementary Materials: The following supporting information can be downloaded at: https://www.mdpi.com/article/10.3390/hydrology13120315/s1, Figure S1: Mean silhouette score as a function of the number of clusters k for (a) heatwave events and (b) extreme precipitation events; Table S1: Sensitivity of the trend results to the number of clusters; Table S2: Sensitivity of the classification to the computation of peak area.

Author Contributions: Conceptualisation, M.G. and G.P.; methodology, M.G.; software, M.G.; validation, M.G., H.Y. and R.H.; formal analysis, M.G.; investigation, M.G.; resources, M.G.; data curation, M.G.; writing, original draft preparation, M.G.; writing, review and editing, M.G., H.Y., R.H. and G.P.; visualisation, M.G.; supervision, G.P. All authors have read and agreed to the published version of the manuscript.

Funding: This research received no external funding.

Data Availability Statement: ERA5 hourly reanalysis data are freely available from the Copernicus Climate Data Store at https://cds.climate.copernicus.eu (accessed on 1 July 2026). The event catalogues and analysis code generated for this study are available from the corresponding author upon reasonable request.

Conflicts of Interest: The authors declare no conflicts of interest.

References

1. IPCC. *Climate Change 2021, The Physical Science Basis. Contribution of Working Group I to the Sixth Assessment Report of the Intergovernmental Panel on Climate Change*; Cambridge University Press: Cambridge, UK; New York, NY, USA, 2021.
2. Lionello, P.; Scarascia, L. The relation between climate change in the Mediterranean region and global warming. *Reg. Environ. Change* **2018**, *18*, 1481–1493. [CrossRef]
3. Tramblay, Y.; Somot, S. Future evolution of extreme precipitation in the Mediterranean. *Clim. Change* **2018**, *151*, 289–302. [CrossRef]
4. Fazzini, M.; Bisci, C.; Billi, P. The climate of Italy. In *Landscapes and Landforms of Italy*; Soldati, M., Marchetti, M., Eds.; Springer: Cham, Switzerland, 2017; pp. 29–42.
5. Gentilucci, M.; Barbieri, M.; Burt, P. Climatic variations in Macerata Province, central Italy. *Water* **2018**, *10*, 1104. [CrossRef]
6. ISPRA. *Indicatori Ambientali, Climate*; Italian Institute for Environmental Protection and Research: Rome, Italy, 2025. Available online: https://indicatoriambientali.isprambiente.it (accessed on 15 September 2026).
7. Coumou, D.; Rahmstorf, S. A decade of weather extremes. *Nat. Clim. Change* **2012**, *2*, 491–496. [CrossRef]
8. Santangelo, M.; Althuwaynee, O.; Alvioli, M.; Ardizzone, F.; Bianchi, C.; Bornaetxea, T.; Brunetti, M.T.; Bucci, F.; Cardinali, M.; Donnini, M.; et al. Inventory of landslides triggered by an extreme rainfall event in Marche Umbria, Italy, on 15 September 2022. *Sci. Data* **2023**, *10*, 427. [CrossRef] [PubMed]
9. Gentilucci, M.; Rossi, A.; Pelagagge, N.; Aringoli, D.; Barbieri, M.; Pambianchi, G. GEV analysis of extreme rainfall, comparing different time intervals to analyse model response in terms of return levels in the study area of central Italy. *Sustainability* **2023**, *15*, 11656. [CrossRef]
10. Cassola, F.; Iengo, A.; Turato, B. Extreme convective precipitation in Liguria, Italy, a brief description and analysis of the event occurred on October 4, 2021. *Bull. Atmos. Sci. Technol.* **2023**, *4*, 4. [CrossRef]
11. Diodato, N.; Ljungqvist, F.C.; Bellocchi, G. Fingerprint of climate change in precipitation aggressiveness across the central Mediterranean, Italian, area. *Sci. Rep.* **2020**, *10*, 22062. [CrossRef] [PubMed]
12. Alexander, L.V.; Zhang, X.; Peterson, T.C.; Caesar, J.; Gleason, B.; Klein Tank, A.M.G.; Haylock, M.; Collins, D.; Trewin, B.; Rahimzadeh, F.; et al. Global observed changes in daily climate extremes of temperature and precipitation. *J. Geophys. Res.* **2006**, *111*, D05109. [CrossRef]
13. Russo, S.; Sillmann, J.; Fischer, E.M. Top ten European heatwaves since 1950 and their occurrence in the coming decades. *Environ. Res. Lett.* **2015**, *10*, 124003. [CrossRef]

14. Lo, S.H.; Chen, C.T.; Russo, S.; Huang, W.R.; Shih, M.F. Tracking heatwave extremes from an event perspective. *Weather Clim. Extrem.* **2021**, *34*, 100371. [CrossRef]
15. Toreti, A.; Desiato, F. Temperature trend over Italy from 1961 to 2004. *Theor. Appl. Climatol.* **2008**, *91*, 51–58. [CrossRef]
16. Brunetti, M.; Maugeri, M.; Nanni, T.; Navarra, A. Droughts and extreme events in regional daily Italian precipitation series. *Int. J. Climatol.* **2002**, *22*, 543–558. [CrossRef]
17. Gentilucci, M.; Barbieri, M.; Burt, P.; Fazzini, M. Analysis of rainfall trends and extreme precipitation in the middle Adriatic side, Marche Region, central Italy. *Water* **2019**, *11*, 1948. [CrossRef]
18. Isotta, F.A.; Frei, C.; Weilguni, V.; Percec Tadic, M.; Lassegues, P.; Rudolf, B.; Pavan, V.; Cacciamani, C.; Antolini, G.; Ratto, S.M.; et al. The climate of daily precipitation in the Alps, development and analysis of a high resolution grid dataset from pan Alpine rain gauge data. *Int. J. Climatol.* **2014**, *34*, 1657–1675. [CrossRef]
19. Cavalleri, F.; Lussana, C.; Viterbo, F.; Brunetti, M.; Bonanno, R.; Manara, V.; Lacavalla, M.; Maugeri, M. Hourly precipitation patterns and extremization over Italy using convection permitting reanalysis data. *Nat. Hazards Earth Syst. Sci.* **2026**, *26*, 279–297. [CrossRef]
20. Libertino, A.; Ganora, D.; Claps, P. Technical note, space time analysis of rainfall extremes in Italy, clues from a reconciled dataset. *Hydrol. Earth Syst. Sci.* **2018**, *22*, 2705–2715. [CrossRef]
21. Libertino, A.; Ganora, D.; Claps, P. Evidence for increasing rainfall extremes remains elusive at large spatial scales, the case of Italy. *Geophys. Res. Lett.* **2019**, *46*, 7437–7446. [CrossRef]
22. Gentilucci, M.; Materazzi, M.; Pambianchi, G.; Guerriero, G. Assessment of variations in the temperature rainfall trend in the Province of Macerata, central Italy, comparing the last three climatological standard normals, 1961 to 1990, 1971 to 2000, 1981 to 2010, for biosustainability studies. *Environ. Process.* **2019**, *6*, 391–412.
23. Gentilucci, M.; Djouohou, S.I.; Barbieri, M.; Younes, H.; Pambianchi, G. Trend analysis of streamflows in relation to precipitation, a case study in central Italy. *Water* **2023**, *15*, 1586. [CrossRef]
24. Salas, J.D.; Obeysekera, J. Revisiting the concepts of return period and risk for nonstationary hydrologic extreme events. *J. Hydrol. Eng.* **2014**, *19*, 554–568. [CrossRef]
25. Healy, C.E.; Huser, R.; Opitz, T. Non stationarities in extreme hourly precipitation over the Piave Basin, northern Italy. *Environmetrics* **2025**, *36*, e70051. [CrossRef]
26. Doswell, C.A. Societal impacts of severe thunderstorms and tornadoes, lessons learned and implications for Europe. *Adv. Geosci.* **2007**, *12*, 135–152.
27. White, R.H.; Battisti, D.S.; Skok, G. Tracking precipitation events in time and space in gridded observational data. *Geophys. Res. Lett.* **2017**, *44*, 8637–8646. [CrossRef]
28. Feng, Z.; Leung, L.R.; Houze, R.A.; Hardin, J.; Chen, D.; Guo, J. A global high resolution mesoscale convective system database using satellite derived cloud tops, surface precipitation and tracking. *J. Geophys. Res. Atmos.* **2021**, *126*, e2020JD034202. [CrossRef]
29. Munoz, C.; Wang, L.P.; Willems, P. Enhanced object based tracking algorithm for convective rainstorms and cells. *Atmos. Res.* **2018**, *201*, 144–158. [CrossRef]
30. Russo, S.; Dosio, A.; Graversen, R.G.; Sillmann, J.; Carrao, H.; Dunbar, M.B.; Singleton, A.; Montagna, P.; Barbola, P.; Vogt, J.V. Magnitude of extreme heat waves in present climate and their projection in a warming world. *J. Geophys. Res. Atmos.* **2014**, *119*, 12500–12512. [CrossRef]
31. Zhang, Y.; Zhou, T. Understanding the mechanism for the recurrence of extreme heat events over large spatial domains, a case study of the 2021 Pacific Northwest heatwave. *Geophys. Res. Lett.* **2023**, *50*, e2022GL101690.
32. Hersbach, H.; Bell, B.; Berrisford, P.; Hirahara, S.; Horanyi, A.; Munoz Sabater, J.; Nicolas, J.; Peubey, C.; Radu, R.; Schepers, D.; et al. The ERA5 global reanalysis. *Q. J. R. Meteorol. Soc.* **2020**, *146*, 1999–2049. [CrossRef]
33. World Meteorological Organization. *WMO Guidelines on the Calculation of Climate Normals*; WMO No. 1203; WMO: Geneva, Switzerland, 2017.
34. Gentilucci, M. Global precipitation regimes and seasonal dynamics from IMERG climatology, focus on Europe and Italy. *Water* **2026**, *18*, 1374. [CrossRef]
35. Rosenfeld, A.; Pfaltz, J.L. Sequential operations in digital picture processing. *J. ACM* **1966**, *13*, 471–494. [CrossRef]
36. Snyder, J.P. *Map Projections—A Working Manual; U.S. Geological Survey Professional Paper 1395*; U.S. Government Printing Office: Washington, DC, USA, 1987.
37. Dixon, M.; Wiener, G. TITAN: Thunderstorm Identification, Tracking, Analysis, and Nowcasting—A radar-based methodology. *J. Atmos. Ocean. Technol.* **1993**, *10*, 785–797. [CrossRef]
38. Benhamou, S. How to reliably estimate the tortuosity of an animal's path: Straightness, sinuosity, or fractal dimension? *J. Theor. Biol.* **2004**, *229*, 209–220. [PubMed]
39. MacQueen, J. Some methods for classification and analysis of multivariate observations. In *Proceedings of the Fifth Berkeley Symposium on Mathematical Statistics and Probability, Berkeley, CA, USA*; University of California Press: Oakland, CA, USA, 1967; Volume 1, pp. 281–297.

40. Rousseeuw, P.J. Silhouettes, a graphical aid to the interpretation and validation of cluster analysis. *J. Comput. Appl. Math.* **1987**, *20*, 53–65. [CrossRef]
41. Kaufman, L.; Rousseeuw, P.J. *Finding Groups in Data: An Introduction to Cluster Analysis*; John Wiley & Sons: New York, NY, USA, 1990.
42. Mann, H.B. Nonparametric tests against trend. *Econometrica* **1945**, *13*, 245–259. [CrossRef]
43. Kendall, M.G. *Rank Correlation Methods*, 4th ed.; Griffin: London, UK, 1975.
44. Sen, P.K. Estimates of the regression coefficient based on Kendall's tau. *J. Am. Stat. Assoc.* **1968**, *63*, 1379–1389. [CrossRef]
45. Pedregosa, F.; Varoquaux, G.; Gramfort, A.; Michel, V.; Thirion, B.; Grisel, O.; Blondel, M.; Prettenhofer, P.; Weiss, R.; Dubourg, V.; et al. Scikit-learn: Machine learning in Python. *J. Mach. Learn. Res.* **2011**, *12*, 2825–2830.
46. Virtanen, P.; Gommers, R.; Oliphant, T.E.; Haberland, M.; Reddy, T.; Cournapeau, D.; Burovski, E.; Peterson, P.; Weckesser, W.; Bright, J.; et al. SciPy 1.0: Fundamental algorithms for scientific computing in Python. *Nat. Methods* **2020**, *17*, 261–272. [CrossRef] [PubMed]
47. Wilks, D.S. "The stippling shows statistically significant grid points": How research results are routinely overstated and overinterpreted, and what to do about it. *Bull. Am. Meteorol. Soc.* **2016**, *97*, 2263–2273. [CrossRef]
48. Formetta, G.; Marra, F.; Dallan, E.; Zaramella, M.; Borga, M. Differential orographic impact on sub hourly, hourly and daily extreme precipitation. *Adv. Water Resour.* **2022**, *159*, 104085. [CrossRef]
49. Crespi, A.; Brunetti, M.; Lentini, G.; Maugeri, M. 1961 to 2015 surface air temperature variability and trends across the Italian regions. *Int. J. Climatol.* **2018**, *38*, 2971–2991.
50. Gentilucci, M.; Bisci, C.; Burt, P.; Fazzini, M.; Vaccaro, C. Interpolation of rainfall through polynomial regression in the Marche region (Central Italy). In *The Annual International Conference on Geographic Information Science*; Springer International Publishing: Cham, Switzerland, 2018; pp. 55–73.
51. Deser, C.; Phillips, A.; Bourdette, V.; Teng, H. Uncertainty in climate change projections: The role of internal variability. *Clim. Dyn.* **2012**, *38*, 527–546. [CrossRef]

Disclaimer/Publisher's Note: The statements, opinions and data contained in all publications are solely those of the individual author(s) and contributor(s) and not of MDPI and/or the editor(s). MDPI and/or the editor(s) disclaim responsibility for any injury to people or property resulting from any ideas, methods, instructions or products referred to in the content.